

# The jet and counterjet of 3C 270 (NGC 4261) viewed in the X-ray with *Chandra*

D.M. Worrall,<sup>1</sup> M. Birkinshaw,<sup>1</sup> E. O’Sullivan,<sup>2</sup> A. Zezas,<sup>3,4,5</sup> A. Wolter,<sup>6</sup> G. Trinchieri<sup>6</sup> and G. Fabbiano<sup>5</sup>

<sup>1</sup>*HH Wills Physics Laboratory, University of Bristol, Tyndall Avenue, Bristol BS8 1TL*

<sup>2</sup>*School of Physics and Astronomy, University of Birmingham, Edgbaston, Birmingham B15 2TT*

<sup>3</sup>*Physics Department, University of Crete, 71003 Heraklion, Greece*

<sup>4</sup>*IESL, Foundation for Research and Technology–Hellas, 7110 Heraklion, Greece*

<sup>5</sup>*Harvard-Smithsonian Center for Astrophysics, 60 Garden Street, Cambridge, MA 02138, USA*

<sup>6</sup>*INAF – Osservatorio Astronomico di Brera, via Brera 28, 20121 Milano, Italy*

10 June 2010

## ABSTRACT

The radio source 3C 270, hosted by nearby elliptical galaxy NGC 4261, is the brightest known example of counterjet X-ray emission from a low-power radio galaxy. We report on the X-ray emission of the jet and counterjet from 130 ks of *Chandra* data. We argue that the X-ray emission is synchrotron radiation and that the internal properties of the jet and counterjet are remarkably similar. We find a smooth connection in X-ray hardness and X-ray to radio ratio between the jet and one of the X-ray components within the core spectrum. We observe wedge-like depressions in diffuse X-ray surface brightness surrounding the jets, and interpret them as regions where an aged population of electrons provides pressure to balance the interstellar medium of NGC 4261. About 20 per cent of the mass of the interstellar medium has been displaced by the radio source. Treating 3C 270 as a twin-jet system, we find an interesting agreement between the ratio of jet-to-counterjet length in X-rays and that expected if X-rays are observed over the distance that an outflow from the core would have travelled in  $\sim 6 \times 10^4$  yr. X-ray synchrotron loss times are shorter than this, and we suggest that most particle acceleration arises as a result of turbulence and dissipation in a stratified flow. We speculate that an episode of activity in the central engine beginning  $\sim 6 \times 10^4$  yr ago has led to an increased velocity shear. This has enhanced the ability of the jet plasma to accelerate electrons to X-ray-synchrotron-emitting energies, forming the X-ray jet and counterjet that we see today.

**Key words:** galaxies: active – galaxies: individual: (3C 270, NGC 4261) – galaxies: jets – X-rays: galaxies

## 1 INTRODUCTION

Low-power radio galaxies appear to be tuned such that their average jet kinetic powers, which are dictated by the rate of accretion onto a central supermassive black hole, provide the heating and momentum input required to limit star formation in their host galaxies by keeping the gas hot (e.g., Granato et al. 2004; Kawata & Gibson 2005; Best et al. 2005; Schawinski et al. 2007). This adds to the interest in studying jets and their lifecycles, and one issue of importance in the study of this feedback process is how the kinetic power of individual sources varies with time. Historically the radio emission has been used as a probe. However, the loss lifetimes of electrons responsible for the radiation exceed flow times along many resolvable jet structures, and thus the radiation that is observed holds

only a time-averaged trace of changes to the central power output and local environmental effects along the jet. X-ray studies of low-power radio galaxies came into fruition with *Chandra*, whose arcsec-scale resolution (Weisskopf et al. 2000) supports the common detection of resolved X-ray synchrotron emission from their kpc-scale jets (Worrall, Birkinshaw & Hardcastle 2001). For X-ray emission the electron energy-loss lifetimes are short compared with light travel times over the structures that are detected, and a focus of much current work is therefore the use of X-ray emission as a probe of distributed particle acceleration (see Worrall 2009, for a review).

Most resolved X-ray jets in low-power radio sources correspond to the brighter radio jet only, indicating that the X-rays are not detected without the assistance of relativistic boost-

ing (e.g., Hardcastle, Birkinshaw & Worrall 2001; Pesce et al. 2001; Marshall et al. 2002; Harris, Krawczynski & Taylor 2002; Birkinshaw, Worrall & Hardcastle 2002; Evans et al. 2005; Worrall et al. 2007; Sambruna et al. 2008). While not unexpected, such effects are an unwelcome complication in the interpretation of measurements. A further complication arises where radio sources show gross asymmetries and bends that must largely result from environments that are different on each side of the nucleus. In order to alleviate these effects, we have chosen to study the nearby radio source 3C 270, whose twin jets lie close to the plane of the sky and whose symmetry is largely intact. In this paper we report a deep X-ray observation of its jet and counterjet.

3C 270 is hosted by the nearby elliptical galaxy NGC 4261 ( $z = 0.00746$ , Trager et al. 2000). The galaxy's major-axis extent to 25 B mag arcsec $^{-2}$  is  $244 \pm 12$  arcsec at position angle  $\sim 160^\circ$ , and the ellipticity is 0.11 (de Vaucouleurs et al. 1991, taken from <http://nedwww.ipac.caltech.edu/>). The radio emission extends roughly 520 arcsec at a position angle  $\sim 88^\circ$  (Birkinshaw & Davies 1985), and is symmetrical on the large scale, as seen in Figure 1 where the black contours of radio emission show the brightest parts of the twin lobes. The jet radio emission to the west is somewhat brighter than the counterjet to the east, but the overall morphology suggests that the radio emission is not highly affected by relativistic beaming. Indeed, Piner et al. (2001) have used the apparent speed and the jet-to-counterjet brightness ratio from VLBI images to deduce a jet speed of  $(0.46 \pm 0.02)c$  and an inclination angle of  $\theta = 63^\circ \pm 3^\circ$ .

X-ray emission from NGC 4261 was first detected using *Einstein* (Feigelson & Berg 1983), but the improved resolution of *ROSAT* was required for component separation. Worrall & Birkinshaw (1994) used the PSPC to separate an unresolved nuclear component from resolved emission both spatially and spectrally, attributing the latter to the thermal atmosphere of the source (see also Fig. 1). Further investigation of the thermal component with *ROSAT* and *ASCA* (Davis et al. 1995; Osmond & Ponman 2004; Finoguenov & Jones 2000) found that the gas temperature increased with distance from NGC 4261, with a group atmosphere taking over from interstellar gas at the outer extremities of the radio source. Gas density and temperature profiles assuming spherical symmetry and using the *Chandra* data discussed here appear in Humphrey et al. (2009), and see O'Sullivan et al. (2010) for further discussion of the galaxy and group gas properties.

Improved measurements of the X-ray core using *XMM-Newton* and an earlier 32-ks *Chandra* observation (Sambruna et al. 2003; Gliozzi et al. 2003; Chiaberge et al. 2003; Donato et al. 2004; Zezas et al. 2005) revealed that part of the nuclear emission suffers from high intrinsic absorption, with  $N_H$  several times  $10^{22}$  cm $^{-2}$  (see also Section 3.4) contrary to the common trend towards low intrinsic absorption in radio galaxies whose bolometric luminosities are small compared with their Eddington limits (Evans et al. 2006).

Resolved X-ray emission from both the jet and counterjet were first seen in the earlier *Chandra* observation (Chiaberge et al. 2003; Zezas et al. 2005), showing 3C 270 to be the brightest known example of counterjet X-ray emission from a low-power radio galaxy. The radio jets close to the nucleus on either side are largely undisturbed, and 3C 270 is thus an excellent source for addressing jet physics. In this paper we concentrate on the resolved X-ray jet and counterjet, and their connection with the unresolved nucleus and their surroundings. Based on our results, we suggest that X-ray synchrotron emission in low-power jets may be used not only to ad-

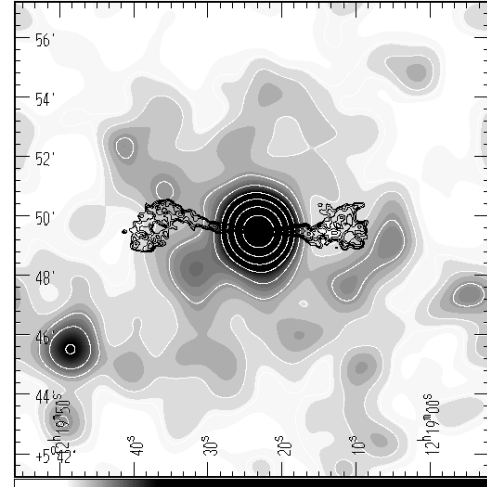


**Figure 1.** Large-scale radio and X-ray structure of NGC 4261. The black contours are of a 5 GHz VLA radio map (Birkinshaw & Davies 1985) made with a  $11.5 \times 10$  arcsec $^2$  beam; the 12 contours are logarithmically spaced between 12 and 220 mJy beam $^{-1}$ . The *ROSAT* PSPC 0.4–2 keV image is smoothed with a Gaussian of  $\sigma = 30$  arcsec. Background has been subtracted and the image is corrected for exposure and vignetting using the EXAS software (Snowden et al. 1994). White X-ray contours, in units of  $10^{-3}$  counts arcmin $^{-2}$  s $^{-1}$ , are 1.1, 1.9, 3.4, 6.0, 11.0, 19.0, 34.0.

dress issues of particle acceleration but also to probe time-variable power released by an active-galaxy nucleus.

We adopt  $H_0 = 70$  km s $^{-1}$  Mpc $^{-1}$ . 1 arcmin corresponds to 9.2 kpc at the distance of NGC 4261.

## 2 *Chandra* X-RAY OBSERVATIONS AND ANALYSIS

We observed NGC 4261 in FAINT data mode with the Advanced CCD Imaging Spectrometer (ACIS) on board *Chandra* on 2008 February 12 (OBSID 9569, sequence 600710). Details of the instrument and its modes of operation can be found in the *Chandra* Proposers' Observatory Guide<sup>1</sup>. Results presented here use CIAO V4.1.2 and the CALDB V4.1.3 calibration database. We recalibrated the data, with random pixelization removed and bad pixels masked, following the software 'threads' from the *Chandra* X-ray Center (CXC)<sup>2</sup>, to make a new level 2 events file. Only events with grades 0, 2, 3, 4, 6 were used, as recommended. After removal of time intervals when the background deviated more than  $3\sigma$  above the average value, the calibrated dataset from 2008 has an observation duration of 100.538 ks.

We had earlier made a shorter observation of NGC 4261 with *Chandra* on 2000 May 6 (OBSID 834, sequence 700139). In 2000 the source was observed with the S3 CCD chip in 512-row subarray and in VFAINT mode, giving a 4 by 8 arcmin field of view. The subarray was used to reduce the readout time to 1.82 s and so decrease the incidence of multiple events arriving from the nucleus within the frame-transfer time (so called pile-up). In the event, we found that pile-up was less than 3% and spectral-fitting results were unaffected (Zezas et al. 2005), and so for our 2008 observations we exposed the whole 8 by 8 arcmin field of the S3 chip, with a frame time of 3.24 s. Some surrounding CCDs were also exposed, but

<sup>1</sup> <http://cxc.harvard.edu/proposer>

<sup>2</sup> <http://cxc.harvard.edu/ciao>

only data from the S3 chip are considered in this paper. The jet was advantageously misaligned with the read-out direction in both observations. To take advantage of the latest calibrations we have also made new level 2 events files for the earlier data, with and without VFaint cleaning to help remove particle background. The calibrated dataset from 2000 has an observation duration of 32.249 ks.

We made a merged events file of the two observations for image-display purposes. For spectral fitting we have extracted data files and calibrations for the two observations separately, and we normally fit them jointly to models. For spectral extraction we use the CIAO task SPEXTRACT, except for the core spectrum where we use PSEXTRACT which is more suitable for a point source, followed by MKACISRMF and MKARF to apply the latest calibrations. For the 2000 data, the core spectrum is extracted from the file where VFaint cleaning has not been applied, since this cleaning removes some events that are likely to be real for a bright point source. Spectra are binned to a minimum of 25 counts per bin for  $\chi^2$  fitting with Gaussian errors using XSPEC. All spectral fitting was performed over the energy range 0.3–10 keV, and includes absorption along the line of sight in our Galaxy assuming a column density of  $N_H = 1.58 \times 10^{20} \text{ cm}^{-2}$  (from the COLDEN program provided by the CXC, using data of Dickey & Lockman (1990)).

Parameter values are quoted with errors corresponding to 90% confidence for one interesting parameter ( $\chi^2_{\min} + 2.7$ , with all other interesting parameters allowed to vary), unless otherwise stated. For non-thermal components, spectral index,  $\alpha$ , is defined in the sense that the flux density is proportional to  $\nu^{-\alpha}$ : the photon spectral index is  $\alpha + 1$ , and the number power-law spectral index of radiating electrons is  $p = 2\alpha + 1$ .

### 3 RESULTS

#### 3.1 Imaging

Our 100-ks *Chandra* exposure reveals more clearly the resolved jet and counterjet, whose presence was noted in the earlier shorter exposure by Chiaberge et al. (2003) and Zezas et al. (2005). From inspection, the jet and counterjet substructures are the same in the two observations and there is no obvious sign of point-like variability. We have therefore combined the data from the two observations. However, our ability to assess variability is limited by the low number of net counts and the strong change in low-energy quantum efficiency of the detector between the observations (see Section 3.3 for more information). Figure 2 shows a false-colour representation of the data. The jet (to the W) and counterjet (to the E) are clearly detected out to 31.7 and 20.2 arcsec, respectively. Both are whiter in colour (i.e., emit relatively more flux above  $\sim 1$  keV) than the galaxy emission, which is asymmetric and flares, particularly to the SW. In both the jet and counterjet the emission appears to be most red (i.e., has the steepest spectrum) furthest from the nucleus (see also Section 3.3). The colour representation shows two point sources, 34.2 and 38 arcsec from the nucleus to the W, and one that is 25.9 arcsec to the E. All three are significantly bluer in colour than either the jet or the diffuse emission in the galaxy, and we do not believe them to be jet features. The jet and counterjet X-ray emission correspond to the regions where the radio emission is brightest, as shown in Figure 3.

Particularly striking in the new data are wedge-like deficits of diffuse X-ray emission around the jet (see also Fig. 4), and to a lesser extent around the counterjet. These are by far the most prominent structural features in the galaxy-scale gas distribution.

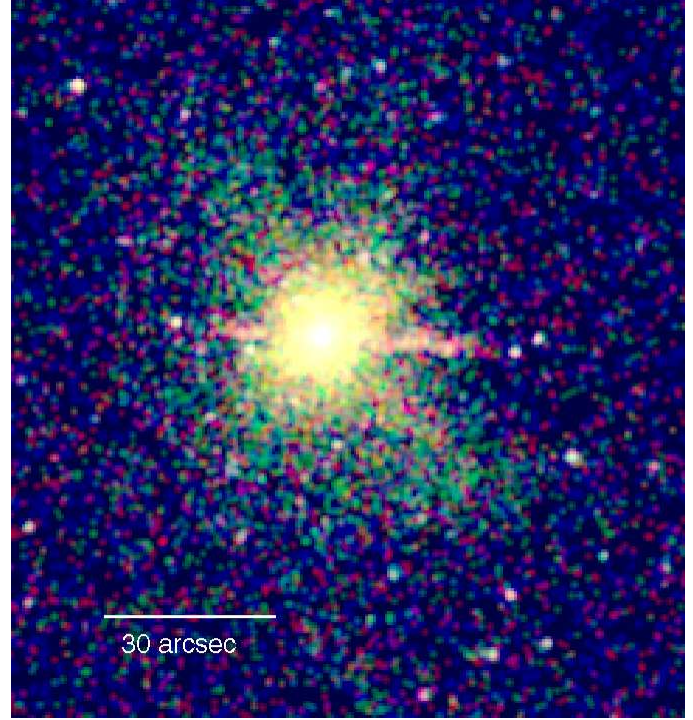


**Figure 2.** False-colour *Chandra* image from the combined *Chandra* observations. Red is 0.3–0.8 keV, green is 0.8–1.2 keV, blue is 1.2–5 keV. The images have each been smoothed with a Gaussian of  $\sigma = 1$  arcsec before being combined.

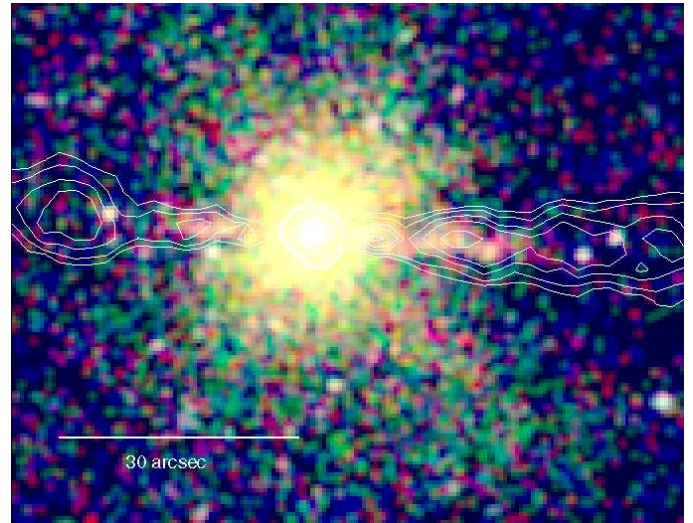


**Figure 3.** Zoomed version of Fig 2 overlaid with contours from a 5 GHz VLA radio map (Birkinshaw & Davies 1985) made with a  $2.3 \times 1.8 \text{ arcsec}^2$  beam; contours at 0.7, 1, 1.5, 2, 3 mJy beam $^{-1}$ .

Their lifetime would be of order the sound crossing time,  $\lesssim 20$  Myr, unless they are maintained. This maintenance could be provided by the radio source, whose overall lifetime is likely to be of order 20 Myr based on forward expansion at several times the speed of sound. The correspondence of these lifetimes and of the wedge geometry with the jet direction would be coincidences if the wedges were temporary features associated with the galaxy encounter suggested by the faint, and almost certainly older, NW tidal

arm reported by Tal et al. (2009). The results therefore suggest that the radio plasma has displaced, transversely, some of the X-ray-emitting atmosphere.

Emission from galaxy gas is prominent in the images, and even in the outskirts of Figure 4 the X-ray emission is largely from gas on the group scale. Many of the point sources in the image are low mass X-ray binaries (LMXBs), and these are discussed in Zezas et al. (2010).

### 3.2 The gas around the resolved X-ray jet

We have compared the emission-weighted temperature of gas in the two wedge-like regions around the jet that are deficient in X-rays (hereafter called ‘wedge gas’) with that of nearby galaxy gas (hereafter called ‘galaxy gas’). The regions are outlined by solid lines in Figure 4, where the triangles sample the wedges and the irregular shapes sample the galaxy gas. In both cases the rectangular region shown in the figure is taken as background: it is within the region where group gas of  $kT \sim 1.3$  keV has been measured (Finoguenov & Jones 2000; Osmond & Ponman 2004; Humphrey et al. 2009).

We have fitted the galaxy gas with a thermal (APEC) model. A contribution from faint unresolved LMXBs is expected, and so we have accounted for this by including a thermal bremsstrahlung component, since that has been found to give a good fit to the cumulative spectrum of the LMXBs of an elliptical galaxy (Sarazin, Irwin & Bregman 2001; Irwin, Athey & Bregman 2003), and has the advantage of being described by just the two parameters of temperature and normalization. The bremsstrahlung temperature is poorly constrained, and following Humphrey et al. (2009) we fix it to  $kT = 7.3$  keV, the well-constrained best fit for 15 nearby early-type galaxies as found by Irwin et al. (2003). The gas abundances are poorly constrained, and so these have been fixed at solar. Our combined model gives  $\chi^2 = 42.8$  for 55 degrees of freedom, as compared with  $\chi^2 = 64$  for no LMXB contribution. The LMXB bremsstrahlung contribution is  $8 \pm 3\%$  of the total 0.3–2 keV luminosity. The galaxy gas has  $kT = 0.63^{+0.03}_{-0.02}$  keV, which agrees with earlier results from *ROSAT*, *ASCA*, *XMM-Newton*, and *Chandra* for roughly this distance from the nucleus (Worrall & Birkinshaw 1994; Finoguenov & Jones 2000; Gliozzi et al. 2003; Zezas et al. 2005; Humphrey et al. 2009). The same model gives a good fit to the wedge gas. The only significance difference (bearing in mind that errors are quoted at 90% confidence) is that the gas temperature is higher in the wedge region, at  $kT = 0.78 \pm 0.09$  keV ( $\chi^2 = 16.6$  for 16 degrees of freedom for the best fit).

In order to test if the special location next to the jet is responsible for the higher temperature in the wedge than in the galaxy gas with which the wedges are partially in contact, we rotated the northern wedge by 90 degrees and the southern by -90 degrees, keeping each vertex the same distance from the nucleus as before (see regions outlined by dashed lines in Fig. 4). While these new regions sample gas at a similar distance from the core than that in the wedges, they miss the brighter plumes of galaxy atmosphere. We found that the rotated wedges gave a similar temperature to that in the wedges surrounding the jet:  $kT = 0.81 \pm 0.05$  keV ( $\chi^2 = 19.8$  for 21 degrees of freedom for the best fit). The emission in the wedge regions is indeed weaker (in the energy band 0.3–2 keV there are  $261 \pm 19$  net counts in the wedges as compared with  $438 \pm 23$  net counts in the rotated wedges). However, we conclude that the gas surrounding the jet is at a typical temperature for its distance from the nucleus. The displacement of gas in the wedge regions is therefore not accompanied by significant local

heating. This is consistent with the absence of edge-brightenings that would suggest supersonic transverse expansion of the cavities, and so implies that these cavities are close to pressure equilibrium with the external gas. The pressure in the cavities can be supplied by the particles and fields in a diffuse radio-emitting plasma that lies around the radio jets but does not appear on the high-frequency and high-resolution radio contour images in Figures 1 and 3 (but see the map in O’Sullivan et al. 2010). The X-ray spectrum of the wedge regions is not inconsistent with this idea: fits incorporating some 0.63 keV gas associated with the inner galaxy atmosphere and 0.9 keV gas associated with the outer atmosphere are permitted in the rotated wedge regions, and the wedge region spectrum can be fitted adequately just with  $\sim 0.9$  keV gas with the same normalization as in the rotated wedge. More precise X-ray spectra would be needed to test this model further.

### 3.3 The X-ray jet and counterjet

We have measured the jet spectrum extracted from a region of position angle 265.5 degrees, width 4.7 arcsec, and length 22.9 arcsec starting at 8.8 arcsec from the nucleus. The counterjet region is defined as being at position angle 85.5 degrees, width 4.7 arcsec, and length 11.5 arcsec, again starting 8.8 arcsec from the nucleus. With the wedge-shaped regions shown on Figure 4 to measure the background, we found that the jet spectrum is fitted by a power law plus a component of thermal emission at  $kT \sim 0.7$  keV. The need for the thermal component was clear in the shape of the residuals, and  $\chi^2$  reduced by 13 when this component was added. This is as expected since the jet extraction region extends closer to the core than the wedge-shaped regions. When we instead sampled the background from regions the same size and shape as the jet and on either side of it, we found a good fit to a power-law component alone. The absorption gave a good fit to the Galactic value, and this was fixed. For the jet, which contains 410 net counts (0.3–5 keV) we found for the power law  $\alpha = 1.22 \pm 0.22$  and, over the band 0.3–5 keV, an unabsorbed flux of  $(1.7 \pm 0.2) \times 10^{-14}$  ergs  $\text{cm}^{-2} \text{s}^{-1}$  and a luminosity of  $(2.1 \pm 0.3) \times 10^{39}$  ergs  $\text{s}^{-1}$ . For the counterjet we used a background region to the north only, since a bluer point-like source lies to the south. The counterjet contains only 149 net counts (0.3–5 keV) and the spectral index is poorly constrained. We found  $\alpha = 0.4^{+0.8}_{-1.1}$  and, over the band 0.3–5 keV, an unabsorbed flux of  $(6.6 \pm 0.8) \times 10^{-15}$  ergs  $\text{cm}^{-2} \text{s}^{-1}$  and a luminosity of  $(8.2 \pm 1.0) \times 10^{38}$  ergs  $\text{s}^{-1}$ .

In the jet region, the 5-GHz radio and 1-keV X-ray flux densities are  $50.3 \pm 1.3$  mJy and  $2.6 \pm 0.2$  nJy, respectively ( $1\sigma$  errors), giving a ratio of  $(1.9 \pm 0.2) \times 10^4$ . The equivalent values for the counterjet are  $13.8 \pm 0.9$  mJy and  $0.8 \pm 0.3$  nJy, with a similar ratio of  $(1.7 \pm 0.6) \times 10^4$ . Figure 5 shows the profiles of X-ray and radio emission in the jet and counterjet in the region where X-ray emission is detected and spatially separated from nuclear and galaxy emission. The subtracted background was sampled locally to each X-ray data point. There is no significant variability in the X-ray emission on the angular scale of these data points between the two observations, which were roughly 8 yr apart, and which are combined to make this plot. However, due to the low numbers of counts we cannot rule out variability of a factor of 2 or less within regions of area 0.3  $\text{kpc}^2$ . The plot is dominated by the 2008 data.

Spectral extraction regions for both the jet and counterjet begin where these features are clearly separated from the point spread function (PSF) of the bright core. If we assume that the jet and counterjet extend into the nucleus with their average measured surface brightness, their estimated 0.3–5 keV total luminosities and



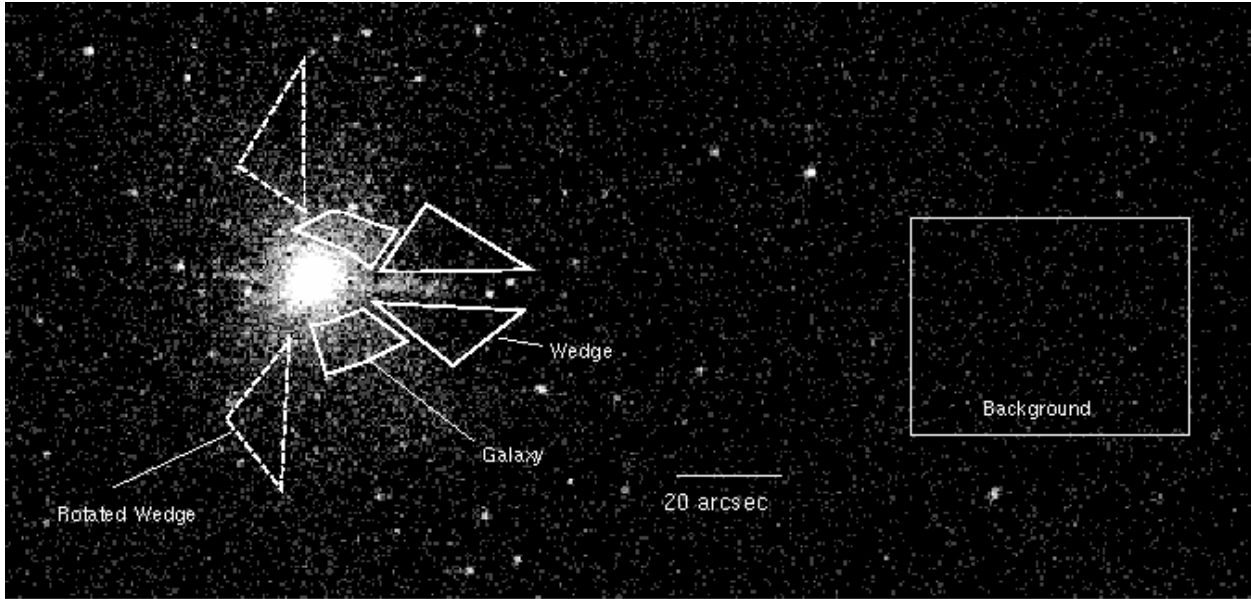


**Figure 4.** 0.3–5 keV unsmoothed X-ray image from the combined *Chandra* observations in 0.492 arcsec pixels overlaid with shapes marking regions used in spectral extraction. The rectangle is the background region for the shapes close to the source. The dashed regions shows the wedges rotated by 90 degrees.

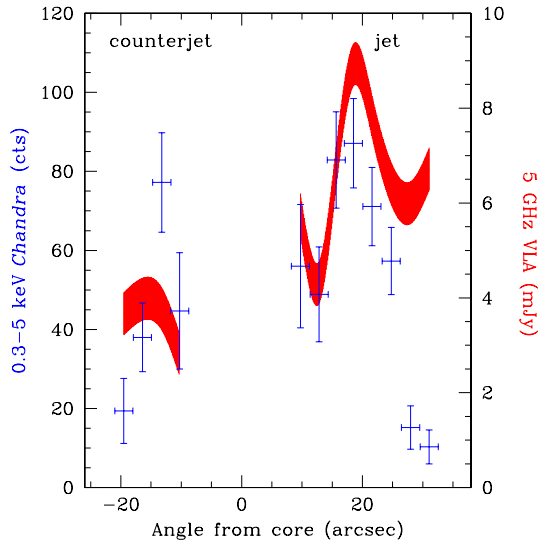


**Figure 5.** Profile of X-ray and radio emission in the jet and counterjet where X-ray emission is detected and spatially separated from other components. The X-ray counts are shown as blue data points with  $\pm 1\sigma$  errors, corresponding to values on the left-hand axis. The radio is measured from the same regions and measurements (corresponding to values on the right-hand axis) are connected with a red band whose thickness corresponds to  $\pm 1\sigma$  errors.

$1\sigma$  uncertainties are  $(2.9 \pm 0.2) \times 10^{39}$  and  $(1.4 \pm 0.1) \times 10^{39}$  ergs  $s^{-1}$ , respectively. Perhaps of more importance is the jet-to-counterjet intensity ratio in the radio and X-ray. For this we should choose identical regions on each side of the nucleus, and so we adopt that of the counterjet and its mirror-image superimposed on the jet. The jet-to-counterjet intensity ratios in the radio and X-ray are then  $1.8 \pm 0.1$  and  $1.6 \pm 0.3$  ( $1\sigma$  errors), respectively. There is some indication from the radio data that the jet-to-counterjet ratio

decreases with distance from the core, as might be expected from a slowing flow. For example, regions of X-ray counterjet length an X-ray-jet's length away give a ratio of  $1.4 \pm 0.1$ . However, our current radio data are not of sufficient quality to explore such issues in depth.

An X-ray hardness-ratio plot (Fig. 6)<sup>3</sup> shows a trend for the X-ray spectrum to get steeper away from the nucleus, but given the statistics the result is not highly significant.

### 3.4 The X-ray nucleus

We extracted the spectrum of the nucleus from a circle of radius 1.23 arcsec. We used background either from a source-centered annulus of radii 2.8 and 8.8 arcsec (as in Zezas et al. 2005) or the rectangular region situated in the group gas. However, none of the interesting parameters in the fits was affected by the choice of background region, and results presented here use only the former region.

In agreement with the results of Zezas et al. (2005) for the earlier, shorter, *Chandra* exposure, we find that in the 2008 data the spectrum requires three components, and our best fit gives a  $\chi^2$  of 114 for 107 degrees of freedom. The first component is a contribution from galaxy gas. The overall fit is insensitive to the abundances, and we set them to solar, with results giving  $kT = 0.61 \pm 0.03$  keV.

The second component is power-law emission of large column density (component PL1). This was found also by others in the earlier *Chandra* or XMM-Newton observations (Sambruna et al. 2003; Gliozzi et al. 2003; Chiaberge et al. 2003; Donato et al. 2004), and its origin is controversially associated either with the accretion flow or the base of the jet (see Zezas et al. 2005). For this heavily absorbed component we find  $\alpha_1 = 0.5^{+0.5}_{-0.3}$ ,  $N_{H1} =$

<sup>3</sup> Calculations using the Bayesian method of Park et al. (2006) (<http://hea-www.harvard.edu/AstroStat/BEHR/>) give essentially the same results.

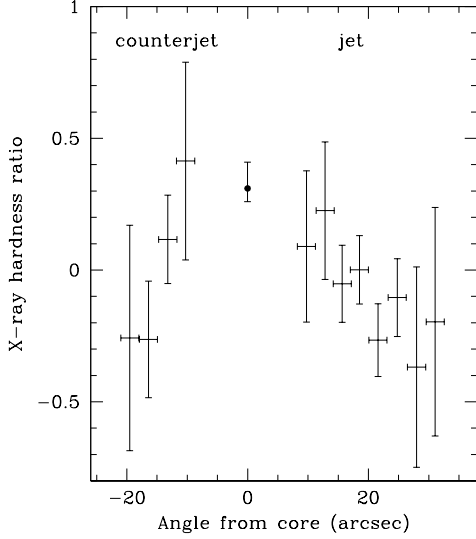


**Figure 6.** Profile of X-ray hardness ratio, defined as  $(H - S)/(H + S)$  where  $H$  is net counts in the band 1–5 keV, and  $S$  is net counts in the band 0.3–1 keV. Errors are  $1\sigma$ . The crosses show values for the jet and counterjet, using neighbouring background regions as described in Section 3.3. The circle corresponds to component PL2 in the core spectrum, extracted as described in Section 3.4.

$6.6^{+2.8}_{-1.9} \times 10^{22} \text{ cm}^{-2}$ , and an unabsorbed 1 keV flux density of  $S_{1 \text{ keV}} = 89^{+110}_{-39} \text{ nJy}$ .

The third is a power law of lower absorption (component PL2). Zezas et al. (2005) pointed out that the UV and optical continuum from the nucleus seen in *HST* data is more likely to be related to this less-absorbed power-law component than to the highly absorbed component as suggested by Chiaberge et al. (2003). We find  $\alpha_2 = 1.1^{+1.9}_{-1.0}$ ,  $N_{H2} = 1.1^{+2.6}_{-1.1} \times 10^{21} \text{ cm}^{-2}$ , and an unabsorbed 1 keV flux density of  $S_{2 \text{ keV}} = 12^{+16}_{-5} \text{ nJy}$ . While the spectral parameters for this soft component are poorly constrained, a fit with only one absorbed power law and a thermal component is unacceptable ( $\chi^2 = 158$  for 109 degrees of freedom). As noted by Zezas et al. (2005), a partial covering model where emission from the nucleus is seen through patchy absorption is an alternative for the combination of PL1 and PL2. However, a partial covering model implies that the emission region is extended on the scale size of the absorbing gas, and it is reasonable to associate the most obscured region with a region of scale-size comparable to the accretion disc and separate it from less absorbed power-law emission.

The parameters for this 3-component model (two absorbed power laws and thermal gas, see Fig. 7) agree within uncertainties with values from the shorter 2000 observation published by Zezas et al. (2005). Weak evidence for a narrow Fe line has been presented by Sambruna et al. (2003), based on *XMM-Newton*, and Zezas et al. (2005), from the 2000 *Chandra* observation. The 2008 observation does not strengthen this case. There is only weak evidence for a line around 6.4 keV in the residuals between the data and the 3-component model (Fig. 7). Formally  $\chi^2$  reduces by just 3 if a narrow line of energy  $6.2 \pm 0.2 \text{ keV}$  (equivalent width  $\sim 131 \text{ eV}$ ) is included.

A combined fit to the 2008 and 2000 *Chandra* data gives similar parameter values to those above, with a fitting statistic of  $\chi^2 = 180$  for 159 degrees of freedom. Freeing up the relative normalizations of the power-law components between epochs yields

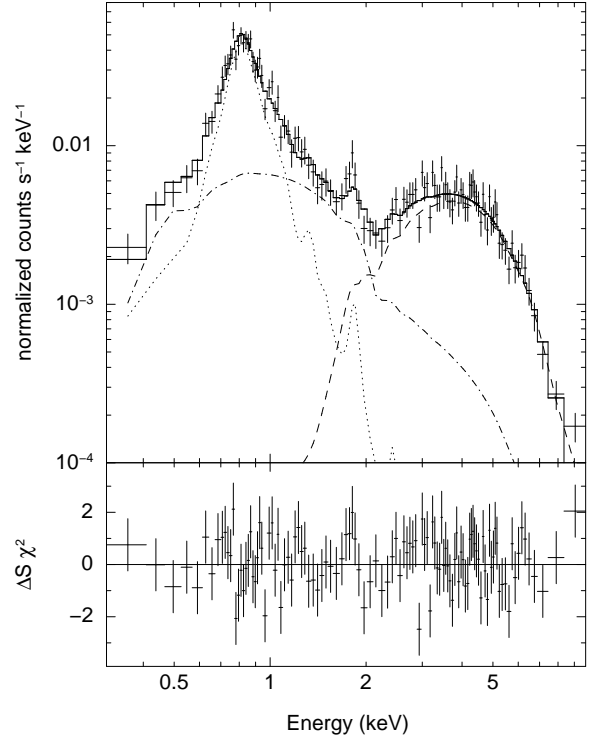


**Figure 7.** Core spectrum from the 2008 *Chandra* observation and best-fit model, with the lower panel showing the residuals as their contribution to  $\chi^2$ . The dashed line is the heavily absorbed power law, the dashed-dotted line is the less absorbed power law, and the thermal contribution is shown as dotted. See text for details.

no significant improvement in fit ( $|\Delta\chi^2| < 1$  for each), and so there is no evidence for variability in either power-law component. In the remaining discussion, when referring to core components we will adopt the parameter values from the combined fit:  $kT = 0.61^{+0.02}_{-0.03} \text{ keV}$ ,  $\alpha_1 = 0.56^{+0.44}_{-0.34}$ ,  $N_{H1} = 7.8^{+2.2}_{-1.9} \times 10^{22} \text{ cm}^{-2}$ ,  $S_{1 \text{ keV}} = 96^{+103}_{-40} \text{ nJy}$ ,  $\alpha_2 = 0.5^{+1.0}_{-0.4}$ ,  $N_{H2} = 2^{+14}_{-2} \times 10^{20} \text{ cm}^{-2}$ , and  $S_{2 \text{ keV}} = 8.5^{+6.1}_{-1.3} \text{ nJy}$ . The 0.3–10 keV intrinsic luminosities for the hard (PL1) and soft (PL2) power-law components are  $1.4 \times 10^{41}$  and  $1.4 \times 10^{40} \text{ ergs s}^{-1}$ , respectively. Note that PL2 contains more than three times the total X-ray luminosity of the resolved jet and counterjet even if they are assumed to extend to pc-scale distances from the nucleus with constant surface brightness.

The core spectrum has been extracted from a circle of radius 190 pc, and it is possible that some of PL2 is contributed by unresolved LMXBs. If the ratio of LMXB X-ray emission to that of the gas is the same as that at kpc distances from the nucleus, based on Section 3.2 we would expect  $8 \pm 3\%$  of the luminosity at 0.3–2 keV (discounting that in PL1) to be from LMXBs, and our model fitting would be folding this into PL2. However, since we measure PL2 to contribute  $39 \pm 4\%$  of the 0.3–2 keV luminosity (again discounting PL1), we consider it unlikely that LMXBs dominate the soft non-gaseous emission. This conclusion is also consistent with the luminosity function of NGC 4261’s LMXBs presented by Giordano et al. (2005). Instead we focus on the evidence that PL2 is jet related.

We note that PL2 is detected in the *Chandra* data but is not separated from thermal emission in the larger PSF of *XMM-Newton*. A nominal extraction circle for point sources in *XMM-Newton* is 30 arcsec in radius, and we can see the issue with ref-

erence to the spectral components in Fig. 7 by recognizing that an *XMM-Newton* extraction would be like scaling the dotted line of the thermal emission up by a factor of  $\sim 600$  relative to the dot-dashed line of PL2. This is a common difficulty for detecting relatively weak soft AGN components with *XMM-Newton*. For a similar reason, the early observations with the still larger PSFs of the *ROSAT* PSPC and *ASCA* did not find that the power-law emission (needed in addition to thermal gas) contains a component that is heavily absorbed.

VLBI mapping of 3C 270 has found a parsec-scale radio jet and counterjet that are well aligned with their kpc-scale counterparts and straddle an unresolved core (Jones & Wehrle 1997). The core has an inverted spectrum and varies in intensity by 30% or more, whereas the pc-scale jet emission is optically thin (Jones et al. 2001; Piner et al. 2001). In observations at 5 GHz taken in 1999 the core had a 5-GHz flux density of  $\sim 80$  mJy while the pc-scale jet and counterjet emission totalled  $\sim 300$  mJy (Jones et al. 2001). In the X-ray, PL1 is ten times more luminous than PL2 but more highly absorbed. It is logical to assume that it arises from a region no larger than the unresolved radio core measured with VLBI. If we then take PL2 as primarily arising from the parsec-scale jet and counterjet, the ratio of radio to X-ray flux density is  $(3.5^{+0.6}_{-2.5}) \times 10^4$ , in agreement with the value of  $\sim 1.8 \times 10^4$  for the kpc-scale structures (Section 3.3). The validity of such a comparison rests on neither radio nor X-ray fluxes having varied by a large factor between measurements taken some years apart. While we cannot be sure of this, particularly since the separation between observations is comparable with the dynamical timescale of the component, we note that no X-ray variability is measured in PL2 over 8 years. In Figure 8 we show the data for the jet and counterjet of Figure 5 in the form of a ratio of X-ray to radio emission, and have added a data-point at the core which uses X-ray counts from PL2 and radio emission from the pc-scale jet and counterjet. Given that PL2 is roughly 40 times brighter than an average jet and counterjet data point, it is remarkable that its ratio of X-ray to radio emission agrees as well as it does with the ratio for the extended emission. This supports the idea that PL2 arises from the pc-scale jet and counterjet through a mechanism similar to that operating on kpc scales.

We have estimated the counts and hardness ratio over 0.3–5 keV for component PL2. To do this we adopted the best-fitting model parameter values and used the *FAKEIT* task in *XSPEC* with appropriate response files and exposures to simulate the counts in the bands 0.3–1 keV and 1–5 keV for the 2008 and 2000 observations, which we then combined. Uncertainties were estimated through further simulations that took into account the uncertainties in the model parameters in the spectral fit. As compared with the jet and counterjet, where bins of width 4.7 arcsec and length 3 arcsec contain less than 100 counts (Fig. 5), PL2 contains  $\sim 1450$  counts. The hardness ratio ( $+0.31$ ) is shown as the filled circle with its error bar in Figure 6. It is noteworthy that the X-ray hardness is comparable to that of the inner parts of the resolved jet and counterjet, lending additional weight to the idea that PL2 represents the bright extension of the jets into the unresolved core. In comparison the thermal emission is much softer: the hardness ratio in the thermal component in the core (using the same method as for PL2) is  $-0.61 \pm 0.03$ , and the galaxy gas in the region defined in Section 3.2 has a hardness ratio of  $-0.51^{+0.03}_{-0.05}$  ( $1\sigma$  errors). Component PL1 is much harder than PL2 due to high absorption, with few counts between 0.3 and 1 keV, and so has a hardness ratio of  $+1.0$ . We emphasize that PL2 has an X-ray hardness ratio that follows the trend seen in the resolved jet.

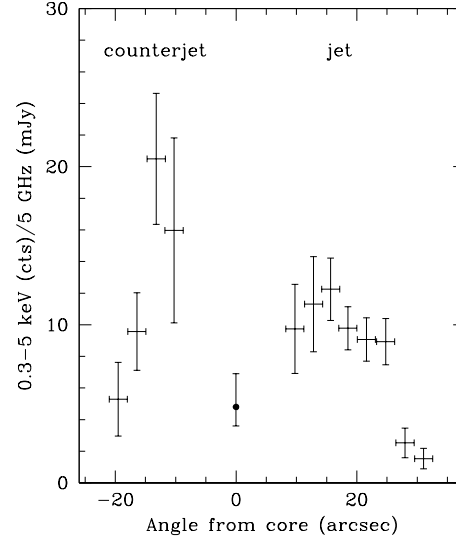


**Figure 8.** Profile of the ratio of 0.3–5 keV X-ray counts to 5 GHz flux density. The data for the jet and counterjet are from Fig. 5. The circle corresponds to X-ray emission from component PL2 in the core spectrum (see Section 3.4) divided by the radio emission from the pc-scale jet and counterjet that are resolved with VLBI.

## 4 DISCUSSION

### 4.1 Emission mechanism of the jet and counterjet X-rays

Here we consider the radio and X-ray emission from the jet and counterjet, as extracted from the regions defined in Section 3.3. A power-law extrapolation to higher frequencies of the radio emission, with a spectral index of  $\alpha_{2.7\text{ GHz}}^{5\text{ GHz}} = 0.56$  (Wall & Peacock 1985), falls above the X-ray emission, but consistency with the X-ray can be found by applying a spectral break,  $\Delta\alpha$ , of similar size in the jet and counterjet. Figure 9 shows the result of applying  $\Delta\alpha = 0.5$ , as expected for the simplest case of continuous injection where the electrons are losing energy by synchrotron radiation and inverse Compton scattering. The predictions for inverse-Compton X-ray emission are insensitive to the form of the electron spectrum at high energies, and we have estimated the minimum-energy magnetic field and the inverse Compton yield assuming a minimum electron Lorentz factor of 10, no heavy particles, and a filling factor of unity (see, e.g., Worrall & Birkinshaw 2006). An inverse-Compton origin for the X-ray emission (from upscattering starlight, see below) suggests an uncomfortably large (factor  $\sim 45$ ) departure from minimum energy, in common with many lower-power jets (e.g., Hardcastle et al. 2001). An inverse Compton origin would also predict similar radio and X-ray spectral slopes, which is allowed by the data for the counterjet but not for the jet. It is therefore highly unlikely that the X-ray emission is of inverse Compton origin, and it is almost certainly produced by synchrotron radiation.

Using the assumptions above and the (weak) level of relativistic beaming with parameters given below (Section 4.5), we find equal minimum-energy magnetic fields in the jet and counterjet (2.2 nT). The spectral break of  $\Delta\alpha = 0.5$  in the synchrotron emission (Fig. 9) is then due to a knee in the electron spectrum at  $\sim 40$  GeV where it breaks from a power-law index of  $p = 2.12$  to 3.12.

Stawarz, Sikora & Ostrowski (2003) pointed out that starlight can be the dominant radiation field for inverse Compton scatter-

ing of electrons in kpc-scale jets, and this is the case for 3C 270 in the region where X-rays are detected. From the V-band surface-brightness profile of Kormendy et al. (2009) we estimate an average starlight energy density for distances between 10 and 20 arcsec from the nucleus of  $9.3 \times 10^{-12} \text{ J m}^{-3}$ , which is to be compared with  $4.2 \times 10^{-14} \text{ J m}^{-3}$  in the cosmic microwave background and  $1.9 \times 10^{-12} \text{ J m}^{-3}$  in minimum-energy magnetic field. In our calculation above of the inverse Compton X-ray contribution from scattering of starlight we have modelled the starlight as peaking at  $10^{14} \text{ Hz}$  (Stawarz et al. 2003) and having a diluted black-body spectrum to match the estimated energy density.

The lifetime of electrons to synchrotron radiation and inverse Compton losses in the Thomson regime,  $\tau$ , is given by

$$\tau = \frac{3m_e c}{4\sigma_T u \gamma}, \quad (1)$$

where  $m_e$  is the electron mass,  $\sigma_T$  is the Thomson cross section,  $\gamma$  is the electron Lorentz factor and  $u$  is the total energy density in photons and field. While it is a simplification to treat the X-ray jet as a single emission region, we can check that  $\sim 40 \text{ GeV}$  (see above) is a consistent break energy in the electron spectrum. Electrons of this high an energy are still just within the Thomson regime for inverse Compton scattering of starlight, and so we use the combined energy density of  $1.1 \times 10^{-11} \text{ J m}^{-3}$  in Equation 1 and calculate a minimum-energy loss lifetime of  $\sim 10^5 \text{ yr}$ . This is comparable to the time ( $\sim 6 \times 10^4 \text{ yr}$ ) that we estimate jet plasma has been flowing along the X-ray-detected jet (Section 4.5), consistent with a model that had the same population of accelerated electrons providing both the radio and X-ray emission through synchrotron radiation.

In Fig. 5 it appears as though the X-ray emission peaks closer to the core (upstream) than the radio. This is seen in other synchrotron jets (e.g. Hardcastle et al. 2001; Dulwich et al. 2007). The X-ray peaks in Fig. 5 must be produced by a series of substructures, since they are broader than the synchrotron loss distance of the emitting electrons convolved with the *Chandra* PSF. By contrast, if synchrotron loss time dictates the size of radio knots, then the radio peaks would be far broader than seen in Fig. 5. Some other process, perhaps expansion, therefore dominates the losses of radio-emitting electrons in knots. But, this is clearly a slow process compared with X-ray loss times, since the radio peaks are wider. The build up of radio surface brightness, from the composite structures, with increasing distance from the core as the plasma flows downstream, is therefore expected to lead to offsets in X-ray and radio surface brightness in the sense observed.

Had X-ray variability been detected between the two *Chandra* observations we would have inferred the presence of components of size a few light years embedded in the jet. While evidence for small features embedded in X-ray synchrotron jets is scarce, it is unmistakable from the flaring of knot HST-1 of M 87 (Harris et al. 2003). More recently, variable X-ray emission is claimed from a light-year scale region of enhanced magnetic field embedded within a knot in the jet of Pictor A (Marshall et al. 2010), a source that had similar-length *Chandra* exposures to 3C 270 but is about 30 times further away. We cannot rule out the existence of such structures within 3C 270 based on our two exposures (Section 3.3) but, relative to Pictor A, these observations are handicapped by the shorter jet and richer X-ray emitting atmosphere.

The X-ray to radio flux-density ratios for the jet and counterjet (Section 3.3) correspond to a two-point spectral index of  $\alpha_{\text{rx}} \sim 0.95$ . This is somewhat steeper than typical values of 0.9

or flatter that are reported for one-sided synchrotron jets at smaller angles to the line of sight (e.g., Worrall et al. 2001; Hardcastle et al. 2001; Worrall et al. 2007). The result can be understood, at least qualitatively, in the context of synchrotron spectra which break and steepen between the radio and X-ray (e.g., Fig. 9) at a fixed frequency in the source frame: the emission from two-sided jets is relatively less blueshifted from Doppler beaming, and so emission at fixed observing frequencies arises from higher frequencies in the source rest frame, and a steeper  $\alpha_{\text{rx}}$  should be measured.

## 4.2 Jet components in the X-ray nucleus

In Section 3.4 we pointed out that the ratio of X-ray emission in PL2 to resolved pc-scale radio emission is similar to that in the jet and counterjet (see also Fig. 8). We used this to support the idea that PL2 is the pc-scale extension of the kpc-scale X-ray jet and counterjet. The small component of intrinsic absorption that is measured is consistent with the pc-scale emission lying within the few-hundred-pc-scale dust disc detected with *HST* (Ferrarese, Ford & Jaffe 1996). The reddening on appropriately small scales is uncertain due to subtraction of the bright optical nucleus, but elsewhere within the disc  $A_v$  is in the range 0.3–0.6 mag (Ferrarese 1999, private communication), leading to a column density in the range of 8 to  $16 \times 10^{20} \text{ cm}^{-2}$  if we adopt the relationship between reddening and hydrogen column density given by Burstein & Heiles (1978). The result is consistent with the hydrogen column found for PL2 of  $2_{-2}^{+14} \times 10^{20} \text{ cm}^{-2}$ , although errors are large.

The similarity of X-ray to radio ratio between PL2 and the kpc-scale emission may suggest that PL2 shares the same synchrotron origin as the resolved jet and counterjet. However, for VLBI-scale components, the synchrotron self-Compton (SSC) process is relatively more important in producing X-rays than for VLA-scale components, and so must be considered as a possible emission mechanism. Jones et al. (2001) give an upper limit of  $\sim 1 \text{ mas}$  for the width of the VLBI jet at 10 mas from the core. The true width would need to be about one hundredth of this upper limit for the SSC process to produce the X-ray component PL2 with a minimum-energy magnetic field. For sizes closer to the upper limit, synchrotron radiation must be responsible unless the magnetic energy density is much less than the particle energy density, so that the VLBI-scale jet is far from minimum energy.

While it seems most likely that PL2 is a synchrotron component, the argument can be turned around to infer that the jet width cannot be less than about 0.01 mas if at minimum energy, else the X-ray emission would be exceeded by SSC. Alternatively, the pc-scale jet could be magnetically dominated.

Radio spectra are typically flat in pc-scale jets, and so the similarity in X-ray to radio flux ratio with the kpc-scale jet requires a similar spectral curvature if indeed the X-ray emission from PL2 is of synchrotron origin. There are several uncertainties, but if we adopt a jet width of 1 mas, energy losses from synchrotron radiation (for a minimum-energy magnetic field) exceed those from the dominant inverse Compton processes (scattering on AGN light and SSC). We find a minimum-energy magnetic field of  $\sim 3 \mu\text{T}$ , and from Equation 1 the synchrotron lifetime of electrons of  $\sim 1 \text{ GeV}$  radiating at around the required break frequency of  $3 \times 10^{11} \text{ Hz}$  is roughly 14 yr. This is similar to the travel time along the 10 mas jet at  $0.46 c$  ( $\sim 11 \text{ yr}$ ).

The X-ray emission mechanisms of PL1 and PL2 cannot be determined on the basis of their X-ray spectral slopes which, while similar, have large errors. However, the ratio of PL1 X-ray to VLBI



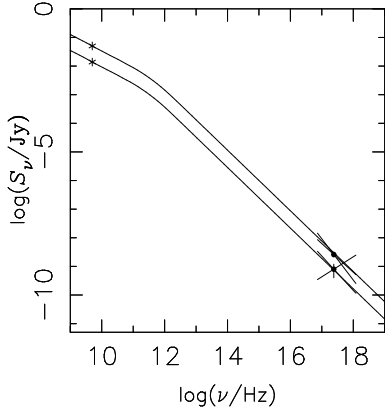


**Figure 9.** Spectral distribution in the radio and X-ray in the jet (upper points) and counterjet (lower points) integrated over regions where resolved X-ray emission is detected. The curves are broken-power-law models,  $\Delta\alpha = 0.5$ , with minimum-energy magnetic fields, and with low-frequency spectra matching a radio spectral index of  $\alpha = 0.56$ .

luminosity is an order of magnitude larger than for PL2. This suggests that if PL1 is embedded in the VLBI core and related to the small-scale jet, the emission mechanism may not be synchrotron. Hardcastle & Worrall (2000) made a statistical argument that if low-power radio galaxies are dimmed, redshifted, versions of BL Lac objects, as suggested by unification models, and the nuclear X-ray emission is related to the base of the radio jet, it must be of inverse Compton rather than synchrotron origin. The radio core in 3C 270 is estimated to be  $\sim 0.02$  mas in radius for its inverted spectrum to be consistent with partial self absorption (Jones et al. 2001). The X-ray emission of PL1 can then arise from the core via the SSC process in a magnetic field of  $\sim 20\mu\text{T}$ , which is roughly 1/5 of the minimum-energy value, if beaming parameters are as for the mas-scale jet. The alternative is that PL1 is dominated by emission from a radiatively inefficient accretion flow (e.g., Zezas et al. 2005).

#### 4.3 Confinement of the kpc-scale jet by the external medium

The pressures in the X-ray-emitting jet and counterjet plasma (Fig. 3) depend on the magnetic-field strengths and particle densities. The minimum pressures correspond to the minimum-energy condition applied above, and give values corresponding to the dashed lines in Figure 10, where we compare with the external gas pressure. The external pressures are from O’Sullivan et al. (2010) (in good agreement with Humphrey et al. 2009) and assume spherical symmetry. The comparison is appropriate if the wedge regions of lower X-ray counts that appear to surround the jet and counterjet (Section 3.2) are in approximate pressure balance with the cooler galaxy gas and with the jet and counterjet with which they are in immediate contact, as suggested by the lack of evidence for supersonically generated features in the gas (for more details see O’Sullivan et al. 2010). From the pressure comparison we can see by how much the jet and counterjet, where X-rays are measured, would have to exceed their minimum pressures to have a dynamical effect on the surrounding gas. Only a small departure from minimum pressure is required for the gentle displacement of wedge gas that appears to have taken place.

Why there is a deficit of counts in wedge-like regions around the jet (and probably also the counterjet) is unclear. The regions would collapse unless there is an unseen component of pressure. It

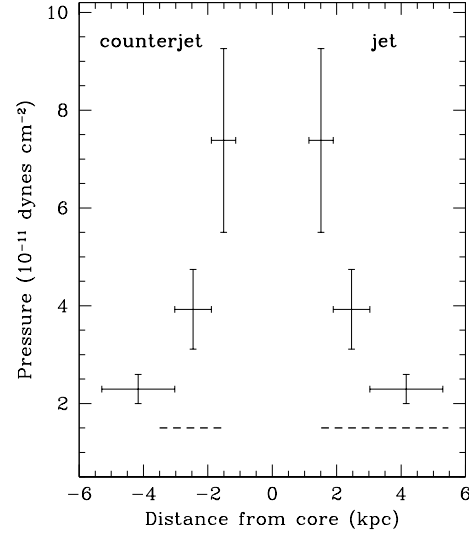


**Figure 10.** The data points (with 90% errors) show the pressure of the external X-ray-emitting atmosphere modelled with spherical symmetry, from the analysis of O’Sullivan et al. (2010). The dashed lines are the deprojected average pressures in the counterjet and jet extraction regions (Section 3.3) assuming minimum energy and modelled as described in Section 4.1. Results suggest that, where resolved X-ray emission is seen, the jet is confined by the external medium and cannot deviate by a large factor from minimum energy.

is most likely that the pressure is supplied by old (lobe) electrons that have lost too much energy to be radiating at 5 GHz or that radiate with too low a surface brightness to be detected without the use of shorter-baseline, lower-frequency, data than used for the image in Fig. 3. (We note that the radio data mapped in Fig. 1 are significant to  $\sim 2.5 \text{ mJy beam}^{-1}$ , a fainter flux density than contoured in the figure, and the lobes then extend much further back towards the jet.) However, we would expect to see only very faint radio emission if any, if the pressure support is from aged electrons since the electron number density at 40 GeV (the energy corresponding to the knee in the jet spectrum of Fig. 9) in a minimum-energy magnetic field would need only to be  $\sim 0.008$  per cent of that in the jet to provide the missing pressure. This assumes that the electron spectrum extrapolates down to Lorentz factors of about unity with an energy-loss spectral index of  $p = 3.12$ .

In the radial analysis of Humphrey et al. (2009), the galaxy and group atmospheres match in density at a radius of about 12 kpc, which is beyond the positions of the wedges. Given that the wedges show a  $\sim 40$  per cent deficit in X-ray emissivity, integrated along the line of sight, as compared with similar regions away from the radio source, we estimate that  $\sim 10$  per cent of the gas mass in the galaxy has been evacuated by the wedges. If the volume occupied by the visible radio structures within the galaxy volume is also taken into account, this increases to  $\sim 20$  per cent of the galaxy gas mass. Thus the radio source is having a significant effect in displacing hot gas within the galaxy, and the work done on the galaxy gas (a few  $\times 10^{50} \text{ J}$ ) will cause appreciable deviations from hydrostatic equilibrium until the work has been thermalized over much of the galaxy atmosphere. Only faint evidence for gas structures is currently seen (O’Sullivan et al. 2010), suggesting that the dynamical processes associated with the development of the radio source were not sudden and violent, and that only weak density and temperature

gradients were created near the cavities containing the radio lobes. Our estimate of the source age,  $\sim 20$  Myr, is too short for stronger structures to have dissipated.

Over a radio source lifetime of  $\sim 20$  Myr, the jet power required to displace the gas is more than  $10^{35}$  W. This is more than our estimates of the broad-band radiative power of the pc-scale and large-scale jets, at  $\sim 8 \times 10^{33}$  W and  $\sim 3 \times 10^{33}$  W, respectively, and more than the unabsorbed X-ray power within the absorbed nuclear component of  $\sim 1.4 \times 10^{34}$  W. From this we infer that the jet radiates less than 20 per cent of its energy. The powers involved are still relatively modest, however, requiring only a small fraction of the Eddington luminosity of the central black hole ( $6.5 \times 10^{39}$  W; Ferrarese et al. 1996).

#### 4.4 Electron lifetime considerations

We argue in Section 4.1 that the kpc-scale X-ray emission is synchrotron radiation. In the minimum-energy magnetic field the synchrotron loss time of X-ray-emitting electrons is of order 800 yr (see equation 14 of Worrall 2009), which is less than the travel time down the 4.9 kpc-long X-ray jet (5.5 kpc de-projected for  $\theta = 63^\circ$ ). In common with other low-power synchrotron jets resolved with *Chandra*, this necessitates particle acceleration to electron energies no less than  $\sim 10^{13}$  eV along the jet.

The mechanism of particle acceleration is not well understood. Some of it may be triggered by the jet interacting with slow-moving gas clouds or high-mass stars as, for example, proposed for some knots in the inner  $\sim 1$  kpc of the jet in nearby Cen A (Hardcastle et al. 2003). However, Cen A is sufficiently nearby to allow proper motions of features in the kpc-scale jet to be measured, and speeds that are a significant fraction that of light are found at radio wavelengths in some knots (Hardcastle et al. 2003). This is inconsistent with those knots being fixed to something travelling at stellar or gas speeds. The jet and counterjet X-ray emission we resolve in 3C 270 is at distances of 1.5 kpc and greater from the core, in the regime where the Cen A jet is distinctly less knotty (Worrall et al. 2008). Furthermore, whereas the host galaxy of Cen A has an inner warped disc suspected to be the merger remnant of a small gas-rich spiral galaxy (e.g., Quillen et al. 2006), there is no reason to believe that NGC 4261 is particularly rich in cold gas or high-mass stars.

Some jets of radio galaxies that are classed as FRI (Fanaroff & Riley 1974) like 3C 270, or are at the low-power end of FRIIs, have features bright in both radio and X-ray that have been identified with strong shocks, largely due to the magnetic-field compression evident in optical polarization data (e.g., Perlman et al. 1999; Dulwich et al. 2007, 2009). However, strong discrete polarization features do not dominate the jet emission of the low-power population as a whole (e.g., Perlman et al. 2006), and a more distributed mechanism of particle acceleration is needed.

Worrall et al. (2008) found that the knotty component of the inner Cen A jet has a flatter X-ray spectrum closer to the jet axis, and used this to support the presence of stratification, with the strongest shear towards the centre of the jet so that stronger turbulence and more efficient particle acceleration might occur there (e.g., as described by Bicknell & Melrose 1982; Eilek & Henriksen 1984; Stawarz & Ostrowski 2002) and migrate to fill the whole width of the jet as a consequence of circulation associated with the shear. Stratified flow is required to explain many of the radio properties of low-power jets (Laing 1996), and in some cases is supported by detailed kinematic modelling (e.g., Laing & Bridle

2002). It may also explain why about 10 per cent of the radio and X-ray emission of the inner jet in NGC 315 is in a filament of oscillatory appearance, possibly representing a magnetic strand caught up in the flow (Worrall et al. 2007). Our assumption in what follows is that in 3C 270 most of the particle acceleration arises as a result of turbulence and dissipation in a stratified flow.

#### 4.5 Jet intermittency?

In Section 3.3 we estimated a radio jet-to-counterjet intensity ratio of 1.8. The ratio due to relativistic boosting is given by  $((1 + \beta \cos \theta)/(1 - \beta \cos \theta))^{(2+\alpha_r)}$ , and so for  $\theta = 63^\circ$  (Section 1) and  $\alpha_r = 0.56$  (Section 4.1), we infer a flow speed of  $\sim 0.25 c$ . This speed is slower than that measured on VLBI scales (Section 1), but is consistent with a jet that is decelerating due to entrainment of material either from the external medium or stellar mass loss (Komissarov 1994). Deceleration is also consistent with the weak evidence above that the X-ray spectrum steepens along the jet, indicative of less kinetic power being available for particle acceleration. However, we note that  $0.25c$  is still highly supersonic with respect to the external medium.

A problem in explaining the jet-counterjet luminosity asymmetry as merely due to relativistic boosting is that the jet and counterjet lengths should be the same, whereas the X-ray jet is detected a factor of 1.56 further from the nucleus than the counterjet. Some of this may be explained by the fact that the jet X-ray surface brightness is higher, and so it can be measured further away. Excluding the faintest two jet points in Figure 5, that would not be detections when de-beamed to the counterjet side, and taking the jet and counterjet as extending into the nucleus, the jet-to-counterjet length ratio is 1.25.

Since the X-ray emission requires *in situ* particle acceleration, a possibility for the length asymmetry is an asymmetry in particle acceleration. However, it is notable that the jet/counterjet length ratio in X-rays matches expectations if the jet and counterjet properties are matched but changed significantly at some time in the past, and X-ray emission is detectable only along the distance that the plasma has travelled ( $\sim 6 \times 10^4$  yr if at  $0.25c$ ) in the time since this change occurred. In this case, the longer light travel time from the counterjet means that we see a shorter counterjet than jet. The sidedness ratio in length is given by  $(1 + \beta \cos \theta)/(1 - \beta \cos \theta) \approx 1.25$ , in agreement with our measurement above.

As to the nature of the change in jet property that occurred  $\sim 6 \times 10^4$  yr ago, we speculate that it might be an increased shear in the jet flow, triggering a higher level of turbulence and dissipation, and corresponding particle acceleration to X-ray energies, and presumably triggered by the very mechanism that launches a jet close to the supermassive black hole. The intermittency of FRII jet central engines over timescales of  $\sim 10^4 - 10^6$  yr has been supported by observational and theoretical considerations (e.g., Clarke et al. 1992; Reynolds & Begelman 1997; Janiuk et al. 2004; Stawarz et al. 2004; Siemiginowska et al. 2007; Kataoka et al. 2008). 3C 270 would then be an example of an FRI displaying a similar behaviour, where we require the intermittency to alter the ability of the jet to accelerate particles to X-ray energies over kpc scales.

If we wish, more globally, to attribute the length of jet seen in X-rays to a process originating from the central engine over a discrete period of time,  $\Delta t$ , we might expect to see examples of detached stretches of X-ray jet along a low-power radio jet. However, there is growing evidence that X-ray emission from low-power jets is not observed beyond a zone of rapid deceleration where the jet

opening angle flares significantly, for example 18 kpc from the nucleus in the case of NGC 315 (Worrall et al. 2007). Given the relatively short time for plasma to reach such a flare point ( $\sim 6 \times 10^5$  yr for NGC 315), the chance of seeing a detached jet would be small unless  $\Delta t$  is typically much shorter than this. Also, where a detached jet is seen it will be interpreted as a knot unless  $\Delta t$  is a large fraction of the time taken to travel to the flare position. A possible example warranting further scrutiny is the long jet of NGC 6251 (Evans et al. 2005), where detached stretches of X-ray emission are seen at (projected) distances of 98–130 and 162–200 kpc from the nucleus (the angle to the line of sight is uncertain).

## 5 CONCLUSIONS

Our *Chandra* observations of 3C 270 have resolved jet emission out to 31.7 and 20.3 arcsec in the jet and counterjet, respectively. The energy spectral index in the jet is  $\alpha = 1.22 \pm 0.22$  (90% errors), with a consistent, but poorly constrained, value for the counterjet. The jet-to-counterjet intensity ratio of  $1.6 \pm 0.3$  ( $1\sigma$  errors) is consistent with that found in the radio, and suggests only modest slowing of jet plasma to about  $0.25c$  from the speed previously inferred on VLBI scales. In common with previous reports for other low-power radio galaxies, we point out that an interpretation of the X-rays as inverse Compton radiation leads to a large departure from minimum energy, and we argue in favour of a synchrotron origin. The jet and counterjet have remarkably similar minimum-energy magnetic fields.

As previously reported, the core X-ray spectrum is complex. However, we find that the X-ray hardness ratio and X-ray-to-radio flux ratio for the kpc-scale emission extrapolate well to match values measured for one of the power-law components measured in the core. We therefore associate this with an inner, bright, extension of the X-ray synchrotron jet. There is weak evidence for the X-ray spectrum of the kpc-scale emission steepening with distance from the core, as would be consistent with slow jet deceleration and reduced kinetic power available for particle acceleration.

We observe wedge-like regions deficient in diffuse X-ray emission surrounding the jets. The regions would collapse under the weight of exterior galaxy and group gas unless there is an unseen component of pressure. We argue that this can be provided by aged electrons from the old radio lobes. Combining the evacuated region with that occupied by the visible jets, we find that the radio source is responsible for having displaced as much as 20 per cent of the mass of the interstellar medium.

The fact that the kpc-scale jet and counterjet are so X-ray bright, internally similar, and apparently undisturbed by their environment, makes their observed properties a powerful probe of the source physics. In particular, while the X-ray jet-to-counterjet luminosity ratio is consistent with an origin in relativistic beaming, the length ratio is not, suggesting instead that it is dictated by light-travel-time effects. This is unexpected, since the synchrotron-loss-lifetime of the X-ray-emitting electrons is short, and *in-situ* particle acceleration must be present. We speculate that the observations can be reconciled if an event in the central engine, starting about  $6 \times 10^4$  yr ago but more recent than the birth of the radio source, increased the ability of the jet to accelerate electrons to energies no less than  $\sim 10^{13}$  eV. This may have arisen through an increased velocity shear enhancing the ability for particle acceleration to proceed through turbulence and dissipation. This suggests that jet X-ray emission in low-power radio galaxies can be used as a probe of the episodic nature of AGN activity. These ideas might

be tested by searching for evidence of other jets in which the X-ray jet length, characteristically shorter than the radio, cannot be explained merely by the jet having rapidly decelerated, and for cases where jet X-ray emission is detached from the core.

## ACKNOWLEDGMENTS

We are grateful to the anonymous referee for suggestions which improved the clarity and completeness of the paper. We thank the CXC for its support of *Chandra* observations, calibrations, data processing and analysis, and the SAO R&D group for DS9 and FUNTOOLS. EOS acknowledges the support of the European Community under the Marie Curie Research Training Network. AZ acknowledges partial support from *Chandra* grant GO8-9094X. Space Astrophysics in Crete is partly supported by EU FP7 *Capacities* GA No206469. This work has used data from the VLA. NRAO is a facility of the National Science Foundation operated under cooperative agreement by Associated Universities, Inc.

## REFERENCES

- Best, P.N., Kauffmann, G., Heckman, T.M., Brinchmann, J., Charlot, S., Ivezić, Ž., White, S.D.M., 2005, MNRAS 362, 25
- Bicknell, G.V., Melrose, D.A., 1982, ApJ 262, 511
- Birkinshaw, M., Davies, R.L., 1985, ApJ, 291, 32
- Birkinshaw, M., Worrall, D.M., Hardcastle, M.J., 2002, MNRAS, 335, 142
- Burstein, D., Heiles, C., 1978, ApJ, 225, 40
- Chiaberge, M., Gilli, R., Macchetto, F.D., Sparks, W.B., Capetti, A., 2003, ApJ, 582, 645
- Clarke, D.A., Bridle, A.H., Burns, J.O., Perley, R.A., Normal, M.L., 1992, ApJ, 385, 173
- Davis, D.S., Mushotzky, R.F., Mulchaey, J.S., Worrall, D.M., Birkinshaw, M., Burstein, D., 1995, ApJ, 444, 582
- de Vaucouleurs, G., de Vaucouleurs, A., Corwin, H.G., Buta, R.J., Paturel, G., Fouque, P., 1991 Third reference catalogue of bright galaxies, Springer-Verlag
- Dickey, J.M., Lockman, F.J., 1990, ARA&A, 28, 215
- Donato, D., Sambruna, R.M., Gliozzi, M., 2004, ApJ, 617, 915
- Dulwich, F., Worrall, D.M., Birkinshaw, M., Padgett, C.A., Perlman, E.S., 2007, MNRAS, 374, 1216
- Dulwich, F., Worrall, D.M., Birkinshaw, M., Padgett, C.A., Perlman, E.S., 2009, MNRAS, 398, 1207
- Eilek, J.A., Henriksen, R.N., 1984, ApJ 277, 820
- Evans, D.A., Hardcastle, M.J., Croston, J.H., Worrall, D.M., Birkinshaw, M., 2005, MNRAS, 359, 363
- Evans, D.A., Worrall, D.M., Hardcastle, M.J., Kraft, R.P., Birkinshaw, M., 2006, ApJ, 642, 96
- Fanaroff, B.L., Riley, J.M., 1974, MNRAS, 167, 31p
- Feigelson, E.D., Berg, C.J., 1983, ApJ, 269, 400
- Ferrarese, L., Ford, H.C., Jaffe, W., 1996, ApJ, 470, 444
- Finoguenov, A., Jones, C., 2000, ApJ, 539, 603
- Giordano, L., Cortese, L., Trinchieri, G., Wolter, A., Colpi, M., Gavazzi, G., Mayer, L., 2005, ApJ, 634, 272
- Gliozzi, M., Sambruna, R.M., Brandt, W.N., 2003, A&A, 408, 949
- Granato, G.L., De Zotti, G., Silva, L., Bressan, A., Danese, L., 2004, ApJ 600, 580
- Hardcastle M.J., Worrall, D.M., 2000, MNRAS, 314, 359

- Hardcastle M.J., Birkinshaw, M., Worrall, D.M., 2001, MNRAS, 326, 1499
- Hardcastle M.J., Worrall, D.M., Kraft R.P., Forman, W.R., Jones, C., Murray, S.S., 2003, ApJ, 593, 169
- Harris, D.E., Krawczynski, H., Taylor, G.B., 2002, ApJ, 578, 60
- Harris, D.E., Biretta, J.A., Junor, W., Perlman, E.S., Sparks, W.B., Wilson, A.S., 2003, ApJ, 586, L41
- Humphrey, P.J., Buote, D.A., Brighenti, F., Gebhardt, K., Mathews, W.G., 2009, ApJ, 703, 1257
- Irwin, J.A., Athey, A.E., Bregman, J.N., 2003, ApJ, 587, 356
- Janiuk, A., Czerny, B., Siemiginowska, A., Szczerba, R., 2004, ApJ, 602, 595
- Jones, D.L., Wehrle, A.E., 1997, ApJ, 484, 186
- Jones, D.L., Wehrle, A.E., Piner, B.G., Meier, D.L., 2001, ApJ, 553, 968
- Kataoka, J., Stawarz, Ł., Harris, D.E. et al., 2008, ApJ, 685, 839
- Kawata, D., Gibson, B.K., 2005, MNRAS 358, L16
- Komissarov, S.S., 1994, MNRAS, 269, 394
- Kormendy, J., Fisher, D.B., Cornell, M.E., Bender, R., 2009, ApJS, 182, 216
- Laing, R.A., 1996, ASP Conference Series 100, 241
- Laing, R.A., Bridle, A.H., 2002, MNRAS, 336, 328
- Marshall, H.L., Miller, B.P., Davis, D.S., Perlman, E.S., Wise, M., Canizares, C.R., Harris, D.E., 2002, ApJ, 564, 683
- Marshall, H.L., Hardcastle, M.J., Birkinshaw, M. et al., 2010, ApJ, 714, L213
- Osmond, J.P.F., Ponman, T.J., 2004, MNRAS, 350, 1511
- O'Sullivan et al., 2010, in preparation
- Park, T., Kayshap, V.L., Siemiginowska, A., van Dyk, D., Zezas, A., Heinke, C., Wargelin, B.J., 2006, ApJ, 652, 610
- Perlman, E.S., Biretta, J.A., Zhou, F., Sparks, W.B., Macchetto, F.D., 1999, AJ, 117, 2185
- Perlman, E.S., Padgett, C.A., Georganopoulos, M. et al., 2006, ApJ, 651, 735
- Pesce, J.E., Sambruna, R.M., Tavecchio, F., Maraschi, L., Cheung, C.C., Urry, C.M., Scarpa, R., 2001, ApJ, 556, L79
- Piner, B.G., Jones, D.L., Wehrle, A.E., 2001, ApJ, 122, 2954
- Quillen, A.C., Brookes, M.H., Keene J., Stern, D., Lawrence C.R., Werner, M.W., 2006, ApJ, 645, 1092
- Reynolds, C.S., Begelman, M.C., 1997, ApJ, 487, L135
- Sambruna, R.M., Gliozzi, M., Eracleous, M., Brandt, W.N., Mushotzky, R., 2003, ApJ, 586, L37
- Sambruna, R.M., Donato, D., Cheung, C.C., Tavecchio, F., Maraschi, L., 2008, ApJ, 684, 862
- Sarazin, C.L., Irwin, J.A., Bregman, J.N., 2001, ApJ, 556, 533
- Schawinski, K., Thomas, D., Sarzi, M., Maraston, C., Kaviraj, S., Joo, S.-J., Yi, S. K., Silk, J.I., 2007, MNRAS 382, 1415
- Siemiginowska, A., Stawarz, Ł., Cheung, C.C., Harris, D.E., Sikora, M., Aldcroft, T.L., Bechtold, J., 2007, ApJ, 657, 145
- Snowden, S.L., McCammon, D., Burrows, D.N., Mendenhall, J.A., 1994, ApJ, 424, 714
- Stawarz, Ł., Ostrowski, M., 2002, ApJ 578, 763
- Stawarz, Ł., Sikora, M., Ostrowski, M., 2003, ApJ, 597, 186
- Stawarz, Ł., Sikora, M., Ostrowski, M., Begelman, M.C., 2004, ApJ, 608, 95
- Tal, T., van Dokkum, P.G., Nelan, J., Bezanson, R., 2009, ApJ, 138, 1417
- Trager, S.C., Faber, S.M., Worthey, G., González, J.J., 2000, AJ, 120, 165
- Wall, J.V., Peacock, J.A., 1985, MNRAS, 216, 173
- Weisskopf, M.C., Tananbaum, H.D., Van Speybroeck, L.P., O'Dell, S.L., 2000, Proceedings of SPIE, Vol 4012, 2
- Worrall, D.M., 2009, A&ARv, 17, 1
- Worrall, D.M., Birkinshaw, M., 1994, ApJ, 427, 134
- Worrall, D.M., Birkinshaw, M., 2006, Lect. Notes Phys., 693, 39
- Worrall, D.M., Birkinshaw, M. & Hardcastle, M.J., 2001, MNRAS, 326, L7
- Worrall, D.M., Birkinshaw, M., Laing, R.A., Cotton, W.D., Bridle, A.H., 2007, MNRAS, 380, 2
- Worrall, D.M., Birkinshaw, M., Kraft, R.P. et al., 2008, ApJ, 673, L135
- Zezas, A., Birkinshaw, M., Worrall, D.M., Peters, A., Fabbiano, G., 2005, ApJ, 627, 711
- Zezas, A. et al. 2010, in preparation